Electrochemical and Solid-State Letters, **2** (10) (1999), PROOF PAGES
S1099-0062(99)05-070-1 CCC: $7.00 © The Electrochemical Society, Inc.

Microvisualization of Structural Features and Ion Electroinsertion Behavior of Patterned WO_3 Thin Films via Integrated Optical and Atomic Force Microscopies

Keith J. Stevenson* **and Joseph T. Hupp**z

Department of Chemistry, Northwestern University, Evanston, Illinois 60208, USA

A new approach for the study of electroinsertion of ions into thin films is presented which utilizes a combination of optical (epi fluorescence) and atomic force microscopies, along with electrochemical techniques. We demonstrate that differential ion/charge transfer reactivity can be temporally and spatially imaged and subsequently correlated with structural characteristics.

Manuscript received May 17, 1999. Available electronicallyAugust XX, 1999.

Metal oxide semiconductor materials (*e.g.*, WO_3, MoO_3, and TiO_2) have shown significant promise for application in the contexts of batteries[1] and electrochromics.[2] In general, these materials are solids that have suitable structural and electronic properties that are able to form insertion compounds by reversible redox reactions together with interfacial ion transfer processes. As indicated by Eq. 1 for WO_3, the double injection of electrons and charge compensating cations (*e.g.*, H^+, Li^+, and Na^+) leads to the stabilization of lower oxidation states. It also leads to intense coloration via long wavelength light absorption

$$W^{VI}O_3 \text{ (transparent)} + xe^- + xM^+ \rightleftharpoons M_xW^{VI-x}O_3 \text{ (blue)} \quad [1]$$

While it is clear that the insertion process involves the transport of both electrons and cations into and through the oxide, the details of the mechanism, and the basis for coloration, remain controversial topics. The latter, for example, has been attributed to intervalence charge transfer from W^{+5} to W^{+6} sites,[3] absorption by electrons trapped at oxygen vacancies,[4] or absorption by small polorons.[5] At a pragmatic level, we seek to utilize the coloration effect to provide for microvisualization of electrochemically stimulated cation insertion and expulsion. We suggest that the ability to construct technologically useful devices can be further improved by adding to our knowledge of *(i)* factors controlling the kinetics of insertion and expulsion, and *(ii)* the influence of film microstructure on device stability and reversibility. Surprisingly, the most effective materials used for reversible ion insertion are inherently disordered, not truly amorphous, and possess morphological inhomogeneities (*e.g.*, atomic-level defects, diverse particle sizes, grain boundaries, and mixed crystallinity). These structural inhomogeneities are suggestive of spatially heterogeneous reactivity which can produce anomalous coloration behavior due to irreversible and nonuniform ion insertion.

Herein, we describe preliminary "microvisualization" studies of structural characterization and electroinsertion behavior of electrochemically deposited WO_3 thin films. We demonstrate that this methodology allows for the study of semiconductor electrode/solution interfaces in which differential ion/charge-transfer reactivity can be spatially and temporally imaged and correlated with high-resolution structural maps. We also show that this methodology is improved considerably by using patterned thin films prepared by microtransfer molding and electrochemical deposition techniques. This allows for a more systematic variation of the film preparation properties and permits localized quantitative surface characterization by atomic force microscopy (AFM) (and additional *ex situ* spectroscopic techniques) by creating a reference registry on the sample.

Experimental

A detailed description of the preparation of patterned metal oxide thin films on transparent, conductive substrates has been described previously.[6] Briefly, a polydimethylsiloxane stamp created from a lithographic master was used to pattern thermally curable epoxy on indium-tin oxide (ITO). A metal oxide "negative" of the pattern was then generated via electrodeposition by cathodic reduction (-0.2 V *vs.* Ag/AgCl) in a aqueous tungsten/hydrogen peroxide solution (~0.1 M). Subsequent oxide sintering in air at 250°C for 2 h produced nearly translucent, strongly adherent films. AFM was performed using a Digital Instruments Multimode Nanoscope IIIa. All measurements were obtained in tapping mode with single etched silicon Nanoprobe SPM tips (cantilever length 125 μm and resonance frequency 307-367 Hz, Digital Instruments). Optical microscopy (fluorescence) studies were performed by using the inverted microscope in an epi fluorescence configuration. A 100 W mercury lamp was used together with a Nikon Plan Fluor (60 X /NA = 0.70) objective, a 365 nm bandpass excitation filter, a 400 nm dichromic mirror and a 450 ± 65 nm bandpass emission filter. Digital images were acquired at 16 s time intervals with 60 ms integration times using an intensified, precooled (-25°C) charge-coupled device (CCD) camera (PentaMax, Princeton Instruments, Inc.). Image analysis and processing (flatfielding and background subtraction) were conducted using software supplied by Princeton Instruments (WinView/32), Empix Imaging, Inc. (Northern Eclipse, version 5.0), and Scion Corporation (Scion Image, version Beta 3b). Electrochemical measurements were made by using a BAS potentiostat (model CV-27) and a Houston Instruments X-Y recorder. A home built, one-compartment, three-electrode Kel-F cell that mounted on the translation stage of the microscope was used for simultaneous optical and electrochemical measurements. Patterned WO_3 thin films on ITO served as the working electrode; Pt wire and Ag/AgCl (BAS, 3 M NaCl) were employed as the counter and reference electrodes, respectively. The electrochemical/optical experiments were conducted at room temperature (25 ± 2°C) in deionized water containing 0.1 M NaCl and 6 mM H_2SO_4, with 7-hydroxycoumarin (~0.5 mM, Aldrich) added as a fluorescent imaging agent.

Results and Discussion

Figure 1 shows a representative, large scale 85 x 85 μm AFM image of a patterned WO_3 thin film fabricated by the microtransfer molding and electrodepostion procedure described in Ref. 6. Excellent array replication with limited pattern distortion (<5 %) is observed and the regularity of this array was maintained over ~25 mm^2 (~33,000 squares). Figure 1b shows an AFM height image of a single patterned square, demonstrating that the films are uniform and homogenous with regard to surface topography and thickness. A higher resolution AFM image (500 x 500 nm area) of the sintered WO_3 microstructure is shown in Fig. 2, indicating that films are amorphous, at least on a micrometer scale, and comprised of roughly spherical particles ranging in size from 15 to 95 nm. This morphology is consistent with that previously reported for electrochemically deposited films of WO_3.[7]

The templating of thin films is also extremely useful for examining morphological changes induced by the sintering process. Since films are patterned they can be indexed to a grid which serves as ref-

* Electrochemical Society Student Member.
z E-mail: jthupp@chem.nwu.edu

Electrochemical and Solid-State Letters, **2** (10) (1999), PROOF PAGES
S1099-0062(99)05-070-1 CCC: $7.00

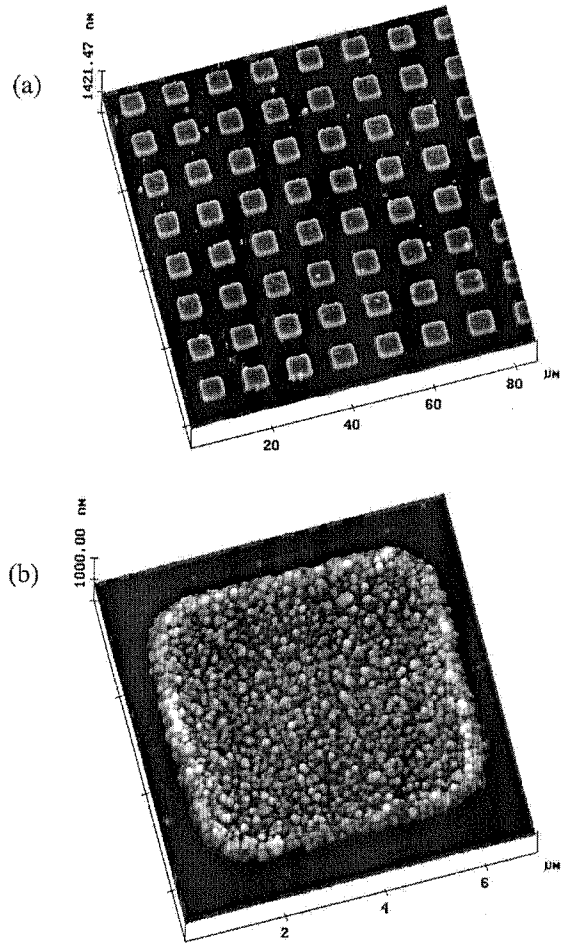

Figure 1. (a) An 85 x 85 μm AFM height image of a patterned WO_3 thin film on ITO prepared via microtransfer molding and electrochemical deposition methods. (b) A higher resolution AFM height image (7 x 7 μm area) of a single patterned square.

erence registry for pre- and postsurface characterization by *ex situ* methods (*e.g.*, AFM, X-ray photoelectron spectroscopy, and energy dispersive X-ray analysis). Analysis of AFM images (data not shown) acquired on the same single patterned WO_3 square before and after sintering at 250°C in air for 2 h indicate that an ~10% decrease in film thickness occurs. In addition, the measured root-mean-square surface roughness for these films was observed to decrease by ~30%. Presumably, these thermally induced structural changes are due to the loss of weakly coordinated water from the WO_3 film, resulting in film densification. These structural changes can significantly alter the ion insertion/expulsion kinetics since heat-treatment can substantially change film porosity and active surface area.

Previously, we have described a series of novel optical imaging experiments for the study of interfacial chemical and electrochemical processes by collecting light from a luminescence producing reaction or probe with an imaging detector (charge-coupled device).[8] In this study, we employ a similar imaging strategy to investigate the electroinsertion behavior of patterned WO_3 thin films in aqueous environments. An illustrative representation of the experimental methodology is shown in Fig. 3. By utilizing the fluorescence from an illuminated solution-phase dye to provide image contrast, changes in the optical density (film absorbance) due to electrochemical reduction can be monitored. The effectiveness of this methodology is particularly enhanced by using patterned substrates, since this helps to provide differential image contrast and allows for

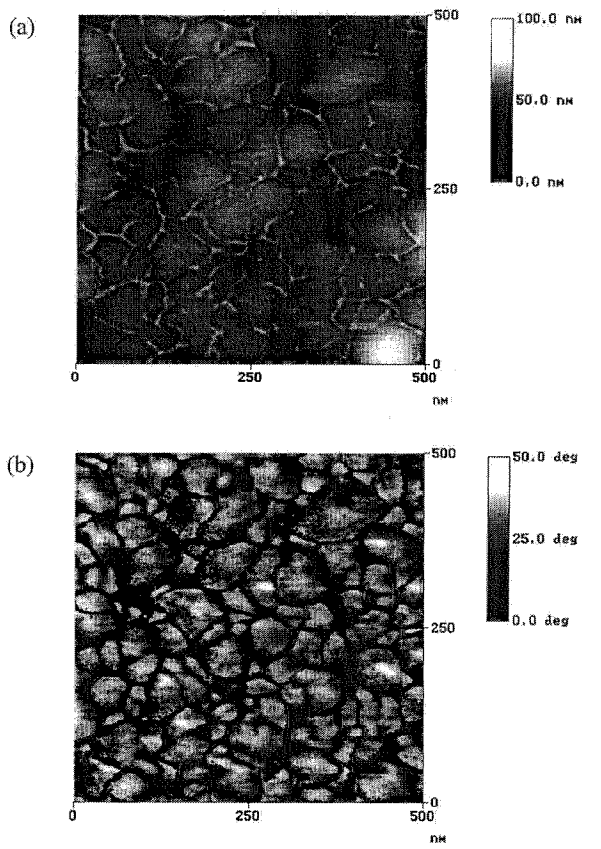

Figure 2. (a) AFM height image (500 x 500 nm area) showing local microstructure of a patterned WO_3 thin film. (b) Simultaneously acquired AFM phase image showing clearer distinction of grain boundaries and definition of component particle grain size.

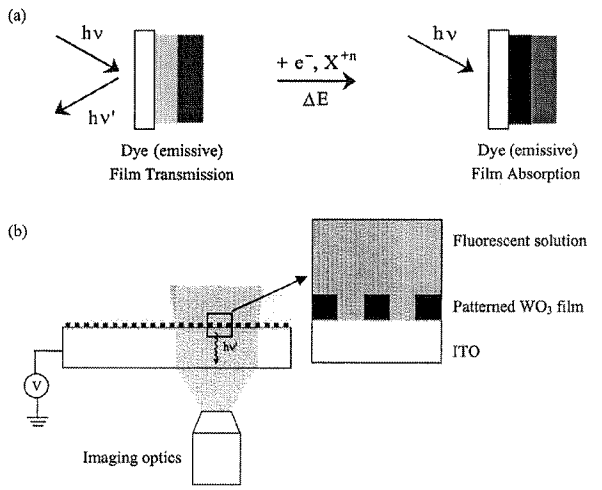

Figure 3. (a) Illustrative representation of the experimental optical microscopy (epi fluorescence) approach employed which is based on utilization of a solution-based fluorescence dye and inner filter film absorbance. The localized electrochromic activity is spatially imaged by the decrease in fluorescence intensity due to film absorbance. (b) Schematic illustration of experimental setup for monitoring the electrochromic reaction of a patterned WO_3 thin film using the approach described above.

S1099-0062(99)05-070-1 CCC: $7.00 © The Electrochemical Society, Inc.

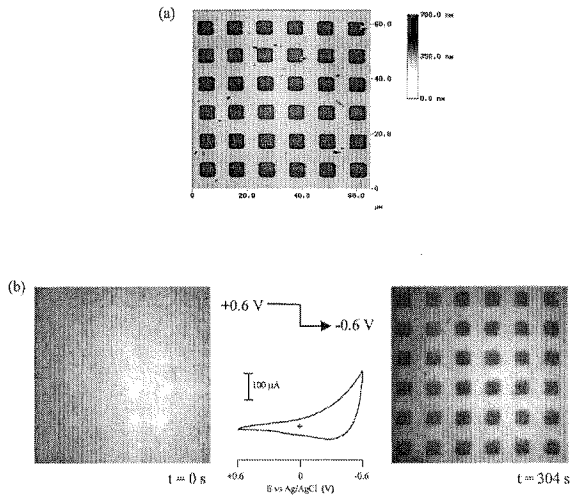

Figure 4. Real-time imaging experiment showing electrocoloration of a patterned WO_3 thin film on ITO immersed in an aqueous solution containing 0.1 M NaCl, 6 mM H_2SO_4 (pH 2.2) and 0.5 mM 7-hydroxycoumain (fluorescent imaging dye). (a) AFM image (65 x 65 μm area) of the patterned WO_3 thin film. (b) Optical imaging experiment (same location) showing the intercalation of protons during reduction of the film as the potential is jumped from +0.6 to -0.6 V *vs.* Ag/AgCl. Total elapsed time is 304 s. For reference, the steady-state cyclic voltammogram of the film is shown in the center.

quantitative calibration and analysis of the optical images (Fig. 3b).

Figure 4 shows the result of an imaging experiment that is based on this experimental methodology. The film was first examined by AFM to determine the structural characteristics and measure film thickness, as shown in Fig. 4a. This particular film had a thickness of *ca.* 220 nm and structural characteristics nearly identical to those shown in Fig. 1 and 2. In order to evaluate the electroinsertion behavior, the film was mounted in the electrochemical/optical cell and repositioned on the inverted microscope in registry to the previously acquired AFM image. Figure 4b shows the results of a real-time optical imaging experiment. The image on the left in Fig. 4b shows the optical response of the film in an oxidized state (+0.6 V *vs.* Ag/AgCl), indicating initial film transparency prior to insertion/coloration. In contrast, Fig. 4b (right) shows the optical response after electrochemical reduction of the film by applying a constant potential (-0.6 V) for 304 s. Nearly uniform insertion, as evidenced by nearly uniform coloration of the patterned WO_3, is clearly observed. The steady-state cyclic voltammogram of the patterned film, acquired after completion of the time-dependent studies, is shown in the center of Fig. 4b. The insertion ratio or mole fraction (x) of injected protons can be estimated from the voltammetric response by integration of the inserted charge (Q). The value of x is calculated from the relationship

$$x = (QM/F\rho dA) \qquad [2]$$

where Q is the injected charge, M is the molecular weight (231.85 g/mol), ρ is the density (7.16 g/cm^3), d is the film thickness, F is Faraday's constant, and A is the area of the patterned array. Substitution of the appropriate parameters yields an insertion ratio of 0.74, indicating that a large number of protons are injected into the film.

A better visualization of the time-dependent insertion/coloration process is presented graphically in Fig. 5. For clarity, the measured decrease in fluorescence intensity due to film absorbance is plotted as an increase, which we term coloration intensity. Cross-sectional profiles of coloration intensity *vs.* distance are shown in Fig. 5a, which correspond to measurements taken across the midpoint of two patterned squares as a function of time. Clearly, differential electrochromic reactivity can be spatially and temporally imaged on micrometer-sized length scales with good sensitivity.

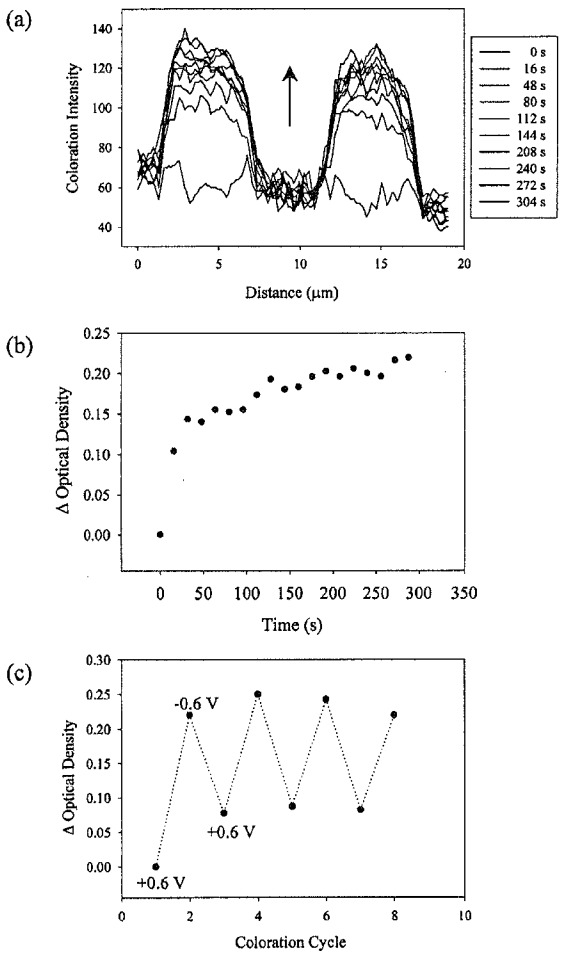

Figure 5. (a) Time-dependent cross-sectional plots of coloration intensity *vs.* distance measured across two patterned WO_3 squares during electrochemical reduction (-0.6 V *vs.* Ag/AgCl). (b) Plot of optical density *vs.* time for a single patterned WO_3 square. (c) Plot of optical density *vs.* coloration cycle for a single WO_3 square. Analysis of data contained in this plot indicates that ~30% of the patterned film remains irreversibly colored after the first cycle.

A more quantitative estimate of the coloration process is obtained by converting the coloration intensity into film transmission and calculating the change in optical density (OD) using

$$\Delta OD = \log(T_o/T_q) \qquad [3]$$

where T_0 is the initial transmission and T_q is the measured time-dependent transmission as the film is reduced by charge insertion. Figure 5b shows a plot of the optical density as a function time for a single patterned square. From inspection of the plot, it is evident that the insertion/coloration process is fast, with ~45% of the film coloration occurring within the first 10 s. Apparently, this process is linear at early times, as expected from the Beer-Lambert law and semi-infinite linear diffusion, but at longer times it begins to saturate as the insertion capacity of the film is reached. The fairly large insertion ratio calculated above suggests that the saturation behavior is a reflection of the concentration-dependent diffusivity of protons, although collapse of the semi-infinite linear diffusion assumption must also be a factor. Saturation behavior has been observed previously for Li^+ insertion into WO_3 by Burdis and Siddle,[9] where they found the behavior to be extremely sensitive to film thickness and film deposition conditions.

The reversible electrochromism (colorless-blue) of the film was

S1099-0062(99)05-070-1 CCC: $7.00

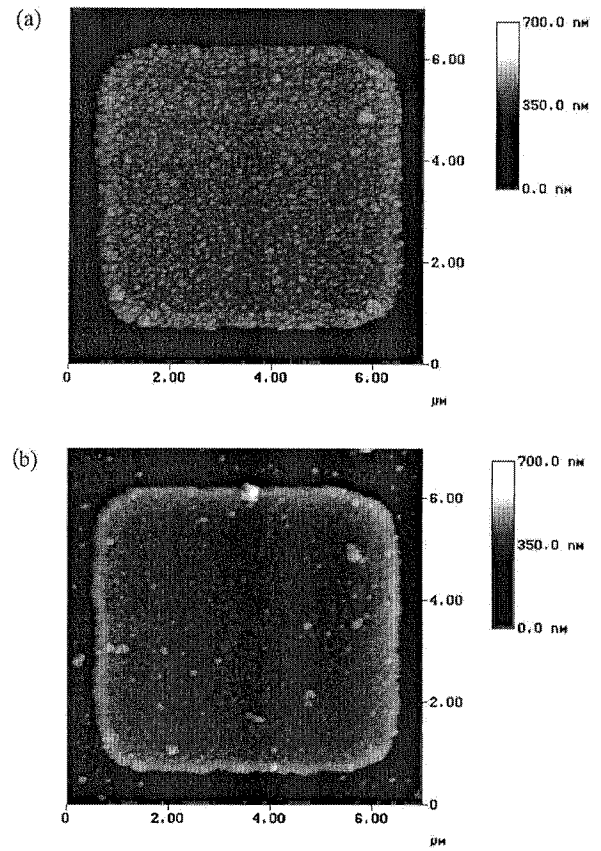

Figure 6. *Ex situ* AFM images (7 x 7 μm area; identical location) of a patterned WO_3 thin film (a) before and (b) after electrochemical cycling (~20 cycles) in an aqueous solution containing 0.1 M NaCl and 6 mM H_2SO_4 (pH 2.2). AFM measurements indicate that the film thickness decreased by *ca.* 77 nm (~35%) during the insertion/coloration experiments. However, the sintered edges of the film experienced little change in surface height, suggesting differences in material stability.

investigated by acquiring images after pausing for 5 min at applied potentials between +0.6 and -0.6 V and measuring the optical density. Figure 5c shows a plot of optical density *vs.* coloration cycle obtained from a single WO_3 square. Initially, at +0.6 V, the film is optically transparent; however, when a negative potential is applied (-0.6 V), a significant change in the optical density is observed. Surprisingly, some irreversibility of the insertion/coloration process is observed after the second insertion cycle, where approximately 30% of the film capacity is lost to irreversible ion insertion. Additionally, a small degree of film conditioning is noticed as indicated by the slight upward and then downward curvature of the plot of optical density response *vs.* insertion/coloration cycle.

Finally, the stability of the patterned WO_3 film was investigated by *ex situ* AFM. Figure 6 shows AFM images obtained before and after the optical imaging experiments. These images reveal that significant film degradation occurred after ~20 insertion/coloration cycles. Analysis of the AFM images indicates that the film thickness decreased by ~35%. However, evaluation of other regions on the film reveals that little change in surface structure and film thickness occurs. This suggests that even parallel microarray processing techniques produce films with a significant degree of inhomogeneity. Presumably, the localized stability of the patterned WO_3 thin films is significantly influenced by microstructural differences (porosity and component particle size) in addition to variations in the amount of lattice-coordinated and weaklyassociated water.

Conclusion

A versatile method for preparing templated tungsten metal oxide thin films on transparent, conductive ITO is demonstrated. In addition, the patterned thin films also serve as quantitative experimental platforms for the study of interfacial ion transfer reactions. A preliminary study has shown that differential electroinsertion/electrochromic activity can be correlated with structural characteristics of patterned WO_3 thin films. A more dramatic and detailed account of the influence of structural features (*i.e.,* film morphology, crystallinity, and film thickness) on the kinetic and optical electroinsertion behavior of redox-active metal oxides, specifically for MoO_3, using our integrated "microvisualization" approach will be presented elsewhere.

Further studies should provide insight into the detailed dynamics and kinetics of ion insertion into redox-active metal oxides, which will yield essential information for the design and understanding of high area, high efficiency electrochemical systems, including state-of-the-art energy storage and energy conversion systems (*e.g.,* metal oxide batteries and electrochromic systems).

Acknowledgment

We gratefully acknowledge the Office of Naval Research for financial support.

Northwestern University assisted in meeting the publication costs of this article.

References

1. M. Winter, J. O. Besenhard, M. E. Spahr, and P. Novak, *Adv. Mater.,* **10**, 725 (1998).
2. C. G. Granqvist, *Handbook of Inorganic Electrochromic Materials,* Elsevier, Amsterdam (1995).
3. R. Faughnan, R. S. Crandall, and P. M. Heyman, *RCA Rev.,* **36**, 177 (1975).
4. S. K. Deb, *Philos. Mag.,* **27**, 801 (1975).
5. O. F. Schirmer, K. W. Blazey, and W. Berlinger, *Phys. Rev.,* **11**, 4201 (1975); O. F. Schirmer, V. Wittwer, B. Baur, and G. Brandt, *J. Electrochem. Soc.,* **124**, 749 (1977).
6. K. J. Stevenson, G. J. Hurtt, and J. T. Hupp, *Electrochem. Solid-State Lett.,* **2**, 175 (1999).
7. K. Yamanaka, *Jpn. J. Appl. Phys.,* **26**, 1884 (1987); E. A. Meulenkamp, *J. Electrochem. Soc.,* **144**, 1664 (1997).
8. K. J. Stevenson and J. T. Hupp, in *New Directions in Electroanalytical Chemistry II,* J. Leddy, P. Vanysek, and M. D. Porter, Editors, PV 99-5, p. 37, The Electrochemical Society Proceedings Series, Pennington, NJ (1999).
9. M. S. Burdis and J. R. Siddle, *Thin Solid Films,* **237**, 320 (1994).